Applicability of ^{99m}Tc-HL91, a Putative Hypoxic Tracer, to Detection of Tumor Hypoxia

Kenji Yutani, Hideo Kusuoka, Kazuki Fukuchi, Mitsuaki Tatsumi and Tsunehiko Nishimura

Division of Tracer Kinetics, Biomedical Research Center, Osaka University Medical School, Osaka, Japan

To elucidate the applicability of ^{99m}Tc-HL91 (HL91) a putative hypoxic tracer, to the imaging of hypoxia in tumors, a biodistribution study of the tracer was performed. The intratumoral distribution of HL91 was compared with that of ^{14}C-deoxyglucose (DG) and the expression of glucose transporter 1 (GLUT1) in an implanted tumor. **Methods:** Biodistribution of HL91 after intravenous injection into Wistar rats with rat mammary tumor (Walker-256) was studied by determining blood and tissue levels of radioactivity from 15 min to 6 h after injection. Dual ex vivo autoradiography was performed on sections of the tumor using HL91 (74 MBq) and DG (185 kBq). The same sections were immunohistologically analyzed with anti-GLUT1 antibody. Tumor tissue was histologically divided into areas of viable cancer cells, necrosis and granulation tissue. The viable cancer cell area was further divided into normoxic and hypoxic areas. Uptake of both tracers in each area was measured quantitatively. The intensity of GLUT1 staining (relative optical density [ROD]) in each area was evaluated by densitometry. **Results:** The uptake of HL91 in the tumor reached a maximal value (0.897 ±0.118% ID [injected dose], mean ±SD, n = 5) at 120 min after intravenous injection of HL91, then gradually decreased. The tumor-to-muscle ratio continued to increase until 360 min (4.34 at 120 min, 7.01 at 240 min and 10.4 at 360 min). HL91 accumulated to significantly higher levels in the hypoxic area than those in the other tissues ($P < 0.0001$). Uptake of DG and expression of GLUT1 were significantly higher in the hypoxic area than in the normoxic area ($P < 0.0001$). In the viable cancer cell area, uptake of HL91 and expression of GLUT1 were strongly correlated (r = 0.624–0.868, mean r = 0.743, $P < 0.0001$), and DG uptake was moderately correlated with GLUT1 expression (r = 0.328–0.669, mean r = 0.505, $P < 0.0001$). **Conclusion:** These results indicate that HL91 can be used to detect tumor hypoxia.

Key Words: ^{99m}Tc; HL91; ^{14}C-deoxyglucose; glucose transporter 1; tumor hypoxia

J Nucl Med 1999; 40:854–861

Heterogeneous perfusion in malignant neoplasms causes regional hypoxia (*1,2*). Hypoxia within a tumor is clinically relevant to radiotherapy and some forms of chemotherapy because it may reduce their effectiveness (*3*). A strong correlation between hypoxia and recurrence rate was reported in advanced cervical cancer (*4*). Therefore, it is important to assess tumor hypoxia before selection of treatment protocols.

Several direct and indirect methods for the measurement of hypoxia have been reported, including oxygen-electrode (*1–4*), magnetic resonance spectroscopy (*5*) and nuclear medicine with radiolabeled bioreductive drugs (*6*). Nitroimidazole-containing compounds have been used to visualize hypoxia in myocardium and tumor tissue (*7–21*). ^{99m}Tc-labeled ligands containing 2-nitroimidazole have been recently developed and show hypoxia selectivity (*22–28*). The recently developed ^{99m}Tc-HL91 (HL91), which lacks the nitroimidazole group, showed even greater hypoxia selectivity (*29*). HL91 demonstrated increased uptake and retention in hypoxic and low-flow ischemic myocardium (*30*), and visualized malignant tumors in a clinical study (*31*).

^{18}F-fluorodeoxyglucose (FDG) has been widely used to visualize malignant tumors. Extensive uptake of FDG and strong expression of glucose transporter 1 (GLUT1) were reported in sites likely to be subjected to hypoxia, and the in vivo uptake of FDG was significantly correlated with GLUT1 antigen staining in a tumor model (*32*). Increases in FDG uptake and GLUT1 expression were observed in HTB77 IP3 cells (in vitro) by exposure to an atmosphere of low oxygen (*33*). Loike et al. (*34*) reported that hypoxia induced GLUT1 messenger ribonucleic acid (mRNA) and protein expression in endothelial cells.

Previous studies (*29–34*) suggest that both HL91 and FDG accumulate to high levels in hypoxic tumor tissue in which GLUT1 is strongly expressed. This study examined the applicability of HL91 for imaging hypoxia in tumors. The relationship between in vivo uptake of HL91 and ^{14}C-deoxyglucose (DG), as well as GLUT1 expression, was evaluated in a tumor model.

MATERIALS AND METHODS

Eight-week-old Wistar rats (female) were subcutaneously injected with a 0.1-mL suspension of 7×10^6 syngeneic Walker-256 tumor cells (rat mammary cancer) in their thighs. When the diameter of the tumor reached about 15 mm (15 ± 2 mm, n = 10, 8 d postinoculation), the following experiments were performed. All experiments were approved by the Animal Research Committee of Osaka University Medical School.

Preparation of HL91

HL91 (Prognox; Nycomed Amersham, Buckinghamshire, England) was prepared by reconstitution of a sterile lyophilized

formulation. Each vial was reconstituted with 1 mL sterile sodium pertechnetate solution containing 370 MBq ^{99m}Tc. Radiochemical purity of each preparation was determined by paper and thin-layer chromatography, and exceeded 95% in all cases.

Biodistribution Study of HL91

HL91 (7.4 MBq) was injected intravenously into tumor-bearing rats. Rats (n = 29) were killed 15, 30, 60, 120, 240 or 360 min after injection. Tissue samples including heart, lung, liver, kidney, blood, muscle and tumor were excised and weighed, and ^{99m}Tc radioactivity was measured with an automated gamma scintillation counter (Gamma Counting Systems; Packard Instrument Co., Meriden, CT). Tissue radioactivity was expressed as the percentage injected dose (%ID)/g tissue. Cross calibration between the gamma counter and a well scintillation dose meter (Deluxe Isotope Calibrator II; Victreen Inc., Cleveland, OH) was performed for ^{99m}Tc.

Biodistribution Study of Deoxyglucose

DG (DuPont NEN, Boston, MA) (37 kBq) was injected intravenously into rats bearing tumors. Rats (n = 26) were killed 15, 30, 60, 90, 120 or 180 min after injection. Tissue samples including heart, lung, liver, kidney, blood, muscle and tumor were excised and weighed. After samples had been completely dissolved in 2 mL tissue solubilizer (Soluene-350; Packard, Downers Grove, IL), 12 mL liquid scintillator fluid (Hionic-flour; Packard) was added to the samples. Radioactivity of the samples was measured with a liquid scintillation counter (model 20101; Wallac Oy, Turku, Finland). Tissue radioactivity was expressed as %ID/g tissue.

Double-Tracer Macro-Autoradiography with HL91 and Deoxyglucose

A total of 74 MBq HL91 and 185 kBq DG were injected into rats (n = 8) with tumors 4 and 1.5 h before killing, respectively. After killing, tumors were quickly dissected, embedded in O.C.T. compound (Miles Inc., Elkhart, IN) and frozen in n-hexane cooled with dry ice. The frozen tissue was sectioned with a cryostat at −20°C. Sections of 5 μm thickness were mounted on a clean glass slide, quickly air-dried with a drier and exposed to an imaging plate (BAS-SR 2025; Fuji Photo Film Co., Ltd., Tokyo, Japan) for 1 h to visualize HL91. One week after initial autoradiography, the same section was exposed to an imaging plate for 3 d to visualize DG. Autoradiographic images were analyzed with a computerized imaging analysis system (Fuji Bio-Imaging Analyzer BAS 5000 Mac; Fuji Photo Film Co.). The pixel size was 50 × 50 μm.

Quantitative analysis of the HL91 autoradiograms was performed using liver samples from normal female Wistar rats as controls. Different doses of HL91 (1.85, 3.70, 7.40, 14.8, 29.6 or 59.2 MBq) were injected intravenously, and rats were killed 30 min later. The liver was excised and divided into two blocks. One block was weighed and ^{99m}Tc radioactivity was measured with an automated gamma scintillation counter. The other was embedded in O.C.T. compound and frozen sections of 5 μm thickness were acquired by the same process as performed on tumors. Liver sections and tumor sections were concomitantly exposed to the same imaging plate. After scanning the plate, the photo-stimulated luminescence (PSL) value was calculated with a computerized imaging analysis system. ^{99m}Tc radioactivity (counts/g) of the liver blocks was plotted against the PSL values of the corresponding liver sections. A standard curve to obtain the %ID/g tissue of HL91 from the corresponding PSL value is shown in Figure 1. ^{99m}Tc radioactivity and PSL values on macro-autoradiograms showed a linear relationship. The %ID was measured within the confirmed
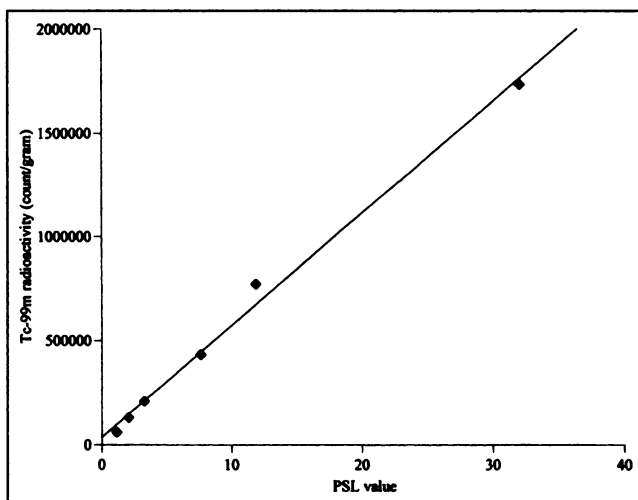

FIGURE 1. Relationship between ^{99m}Tc radioactivity (counts/g) and PSL values on macro-autoradiogram. In experimental dose range, PSL values were linearly related to ^{99m}Tc radioactivity.

range of linearity. The %ID/g tissue of HL91 was calculated and corrected for decay.

Microscales of ^{14}C (Nycomed Amersham) were used to obtain the %ID/g tissue on the autoradiogram of DG.

Immunohistochemistry

After autoradiography, the same section was stained with polyclonal anti-GLUT1 antibody (rabbit anti-GLUT1 AB1340; Chemicon International Inc., Temecula, CA). Paraformaldehyde-fixed paraffin sections (5 μm thickness) of Walker-256 tumors were also stained with anti-GLUT1 antibody. The sections were incubated with anti-GLUT1 antibody, and the bound antibody was visualized with horseradish peroxidase-conjugated antibody (Cappel Organon Teknika Corp., Durham, NC), H_2O_2 and diaminobenzidine. Consecutive sections incubated with normal rabbit IgG were used as negative controls. Sections from paraffin-embedded brain from normal fasted rats were used as positive controls.

Intensities of GLUT1 staining were measured by densitometry using a computer-assisted video densitometry system (MCID system; Imaging Research Inc., St. Catherine's, Ontario, Canada).
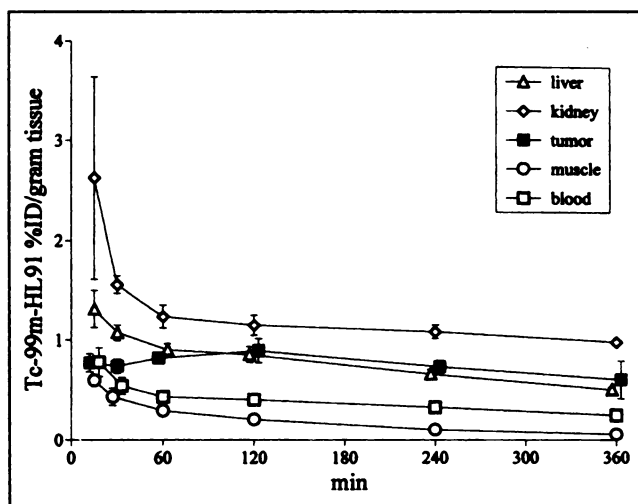

FIGURE 2. Time course of tissue distribution of HL91 using Walker-256 tumor-bearing Wistar rats.

TABLE 1
Tumor-to-Muscle Ratios and Tumor-to-Blood Ratios of ^{99m}Tc-HL91 in Tumor-Bearing Rats

Ratio	Time after injection (min)					
	15 (n = 5)	30 (n = 6)	60 (n = 5)	120 (n = 5)	240 (n = 5)	360 (n = 3)
Tumor-to-muscle	1.29 ± 0.22	1.72 ± 0.14	2.80 ± 0.19	4.34 ± 0.22	7.01 ± 0.35	10.4 ± 0.7
Tumor-to-blood	0.991 ± 0.174	1.37 ± 0.16	1.91 ± 0.23	2.22 ± 0.19	2.25 ± 0.28	2.45 ± 0.25

The relative optical density (ROD) was calculated as follows:

$$ROD = \log_{10} (2^8/\text{observed gray levels}).$$

The RODs of the autoradiograms were measured by the same system to overlay the autoradiograms over the GLUT1-stained frozen section.

Light Microscopic Examination

The Walker-256 tumor tissue was fixed in 4% neutral-buffered paraformaldehyde, dehydrated in graded alcohol and embedded in paraffin. The sections of 5 μm thickness were stained with hematoxylin and eosin, using routine staining procedures for histological characterization.

The tumor tissue was divided into areas of viable cancer cells, large necrosis and granulation tissue by histological examination. A number of focal necrotic areas were scattered in the viable cancer cell area; they appeared as small necrotic foci surrounded by viable cancer cells. The sizes of small necrotic foci varied (112 ± 73 μm, n = 20). The area of large necrosis was defined as the necrotic area. The viable cancer cell layers bordering the necrotic area and surrounding the small necrotic foci were defined as the hypoxic area. The maximum distance from a specific necrotic focus for cancer cells to be designated as belonging to the hypoxic area was 250 μm. Cellular swelling, clumping of the nuclear chromatin or both were morphological characteristics of viable cancer cells in

the hypoxic area. The remaining viable cancer cells (nonhypoxic) occupied the normoxic area. Thus, tumor tissue was divided into four histological categories.

Statistical Analysis

Data are expressed as mean ± SD. Groups were compared by analysis of variance with Scheffé's test. Two correlation coefficients were compared with Fisher Z-transformation and Student paired t test. A value was considered significant when $P < 0.05$.

RESULTS

Biodistribution of HL91

The time course of tissue distribution of HL91 is shown in Figure 2. Uptake of HL91 in the tumor reached a peak at 120 min (0.897 ± 0.118 %ID) and then gradually decreased. Uptake by the kidney was always significantly higher than that by any other tissue ($P < 0.05$). The difference between the tumor uptake and liver uptake at 60 min or later was not significant. HL91 uptake by the heart, lung and muscle, as well as the blood level of HL91 were significantly lower than that of the tumor at 60 min or later ($P < 0.05$). The tumor-to-muscle and tumor-to-blood ratios continued to increase until 360 min (Table 1).
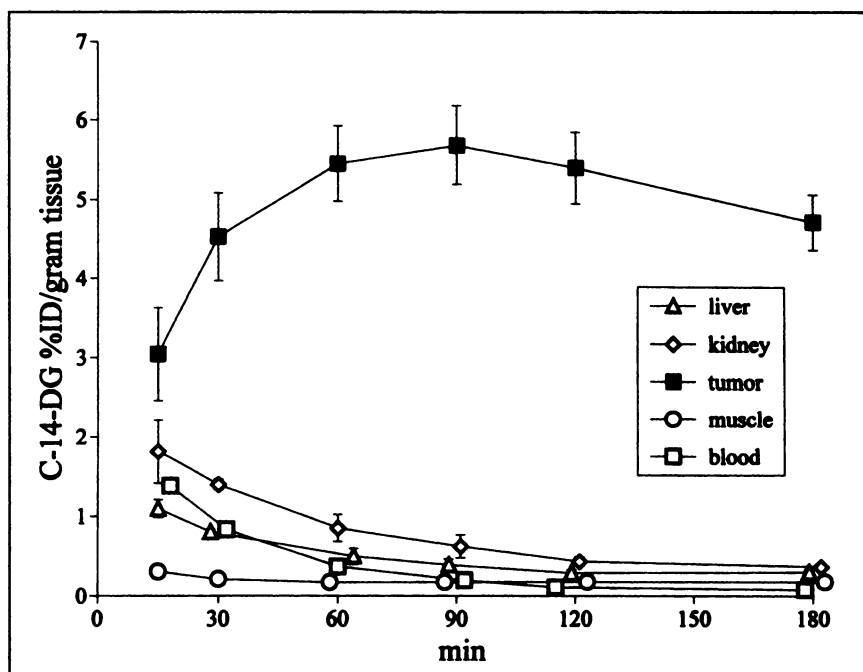
FIGURE 3. Time course of tissue distribution of DG using Walker-256 tumor-bearing Wistar rats.

TABLE 2

Tumor-to-Muscle Ratios and Tumor-to-Blood Ratios of ^{14}C-Deoxyglucose in Tumor-Bearing Rats

| Ratio	Time after injection (min)					
	15 (n = 4)	30 (n = 4)	60 (n = 5)	90 (n = 5)	120 (n = 5)	180 (n = 3)
Tumor-to-muscle	10.4 ± 1.9	22.3 ± 2.6	33.9 ± 4.0	31.1 ± 2.9	26.4 ± 4.8	28.3 ± 2.5
Tumor-to-blood	2.20 ± 0.41	5.39 ± 0.40	15.3 ± 3.1	29.4 ± 5.2	43.1 ± 5.8	65 ± 2.7

Biodistribution of Deoxyglucose

The time course of tissue distribution of DG is shown in Figure 3. Uptake of DG in the tumor reached a peak at 90 min (5.71 ± 0.50 %ID) and then gradually decreased. Uptake by the tumor was always significantly higher than that of any other tissue ($P < 0.05$). The tumor-to-muscle ratios reached a peak at 60 min and then gradually decreased, whereas the tumor-to-blood ratios continued to increase until 180 min (Table 2).

## Distribution of HL91 and Deoxyglucose, and Expression of GLUT1 in Tumor

The autoradiogram of HL91 and DG and the corresponding frozen section stained with anti-GLUT1 antibody are shown in Figure 4. The pattern of uptake of HL91 differed from that of DG, especially in the necrotic area (e.g., area 1 in Fig. 4) in which HL91 uptake was moderate but DG uptake was almost null. In the hypoxic area (e.g., areas 2 and 3 in Fig. 4), HL91 uptake was high and DG uptake was generally high but variable. In the normoxic area, HL91 uptake was low but DG uptake was moderate. GLUT1-positive cytoplasmic granules were observed in most of the viable cancer cells. Intensity of staining was heterogeneous. The highest intensity of staining was seen in the hypoxic area (e.g., areas 2 and 3 in Fig. 4), and moderate staining was seen in the normoxic area. The expression of GLUT1 was similar to the distribution of HL91 in the whole section.

The uptake of HL91 and DG and the amount of GLUT1 in each area are summarized in Figure 5. HL91 and DG accumulated in the hypoxic area to significantly higher levels than in the other tissues ($P < 0.0001$). GLUT1 was also most strongly expressed in cells in the hypoxic area ($P < 0.0001$). In this area, strong expression of GLUT1 was
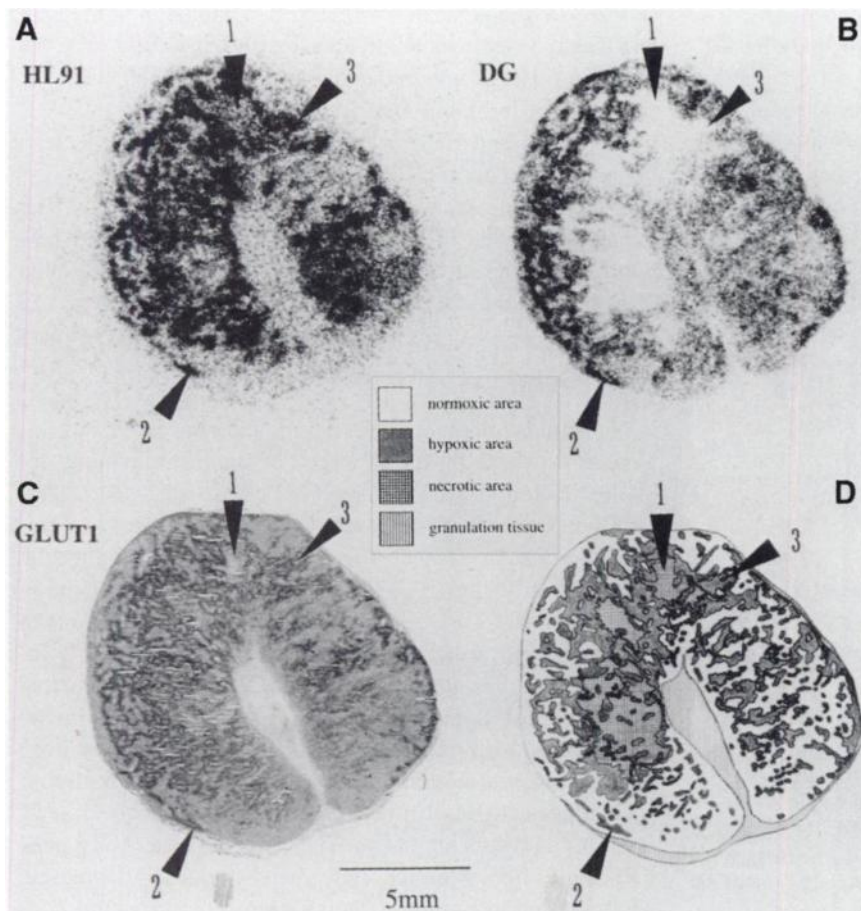

FIGURE 4. Macro-autoradiograms of HL91 (A), DG (B) and corresponding section immunostained with anti-GLUT1 antibody (C). (D) Histological distribution. Arrowhead 1 indicates necrotic area, arrowheads 2 and 3 indicate different types of hypoxic area. DG uptake was high in area 2, but almost null in area 3.
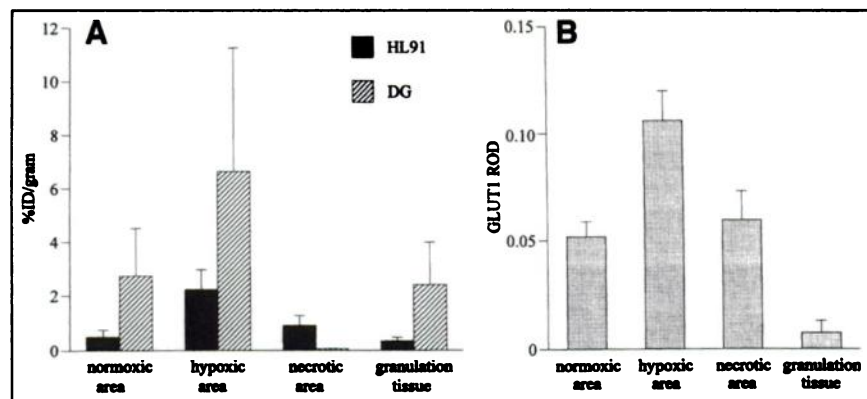
FIGURE 5. Uptake of HL91 and DG (A), and expression of GLUT1 (B) in each area. Uptakes of HL91 and DG were obtained from eight sections of 8 rats. Each section contained 500–1000 regions of interest (ROIs). Total number of ROIs for normoxic, hypoxic and necrotic areas and granulation tissue were 1950, 2520, 1200 and 720, respectively. Amount of GLUT1 was obtained from one section, because ROD is a relative value and cannot be merged with values of other sections. Number of ROIs in normoxic, hypoxic and necrotic areas and granulation tissue were 300, 340, 100 and 70, respectively. Distribution of GLUT1 in other sections was similar to that of section shown in this figure. Each ROI measured 0.062 mm^2.

observed in the cell membranes in addition to the cytoplasmic granules. HL91 uptake by the necrotic area was significantly greater than that of both the normoxic area and granulation tissue ($P < 0.05$). DG uptake by the necrotic area was almost negligible, but moderate DG uptake was observed in the normoxic area and the granulation tissue. GLUT1 expression was moderate in the normoxic and necrotic areas. GLUT1-positive staining in the necrotic area was observed in the necrotic cancer cells and debris. The pattern of GLUT1 expression was similar in paraffin sections to that in the frozen sections (Fig. 6). In paraffin sections of rat brain (positive control), strong staining of endothelial cells lining the blood vessels was observed. In both paraffin and frozen sections of tumor tissue incubated with normal rabbit IgG (negative control), no staining was observed.
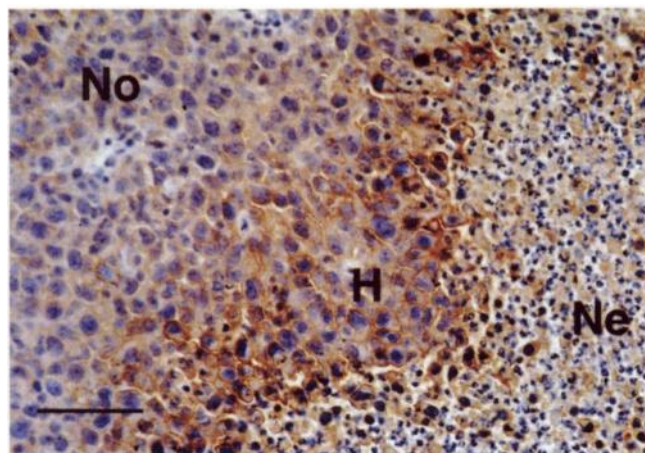

FIGURE 6. GLUT1 expression in Walker-256 tumors stained in paraffin section (×100). Highest intensity of staining is observed in viable cancer cell layers surrounding necrotic area (hypoxic area). Some cancer cells and debris in necrotic area are strongly stained. No = normoxic area; H = hypoxic area; Ne = necrotic area. Bar = 100 μm.

HL91 and DG autoradiograms were overlapped with the GLUT1-stained frozen section using MCID. The ROD in the autoradiogram was compared with that in the corresponding GLUT1-stained section. In the viable cancer cell area (normoxic and hypoxic), the uptake of HL91 was strongly correlated with GLUT1 expression ($r = 0.624$–0.868, mean $r = 0.743$; $P < 0.0001$, n = 8, Fig. 7 and Table 3), and DG uptake was moderately correlated with GLUT1 expression ($r = 0.328$–0.669 mean $r = 0.505$, $P < 0.0001$, n = 8, Fig. 8 and Table 3). In the whole areas of the tumor section, the uptake of HL91 was moderately correlated with GLUT1 expression ($r = 0.460$–0.695, mean $r = 0.607$, $P < 0.0001$, n = 8, Fig. 7 and Table 3), whereas no correlation was seen between uptake of DG and expression of GLUT1 ($r = 0.228$–0.416 mean $r = 0.303$, n = 8, Fig. 8 and Table 3). The expression of GLUT1 was better correlated with HL91 uptake than DG uptake, both in the viable cancer cell area ($P < 0.01$) and in the whole tumor section ($P < 0.005$).

DISCUSSION

Nitroimidazole-containing compounds have been evaluated as markers of tissue hypoxia. Such compounds include ^{18}F-fluoromisonidazole (FMISO) (8,10,11,16,17,21), ^{18}F-fluoroerythronitroimidazole (21), ^{123}I-iodoazomycin arabinoside (IAZA) (19,20) and ^{131}I-iodovinylmisonidazole (12). Recently, the ^{99m}Tc-labeled nitroimidazole-containing compound, BMS181321, has been reported to accumulate in ischemic myocardium and tumor tissue (22–28). ^{99m}Tc-HL91M, which contains a nitroimidazole group, also showed selectivity for hypoxic areas. A complex of core ligand without the nitroimidazole group, HL91, has shown even greater hypoxia selectivity (29), and has been reported to accumulate in hypoxic myocardium and tumor tissue (30,31).

In this study, the uptake of HL91 by tumor reached a peak 120 min after injection and then gradually decreased, whereas tumor-to-muscle and tumor-to-blood ratios con-
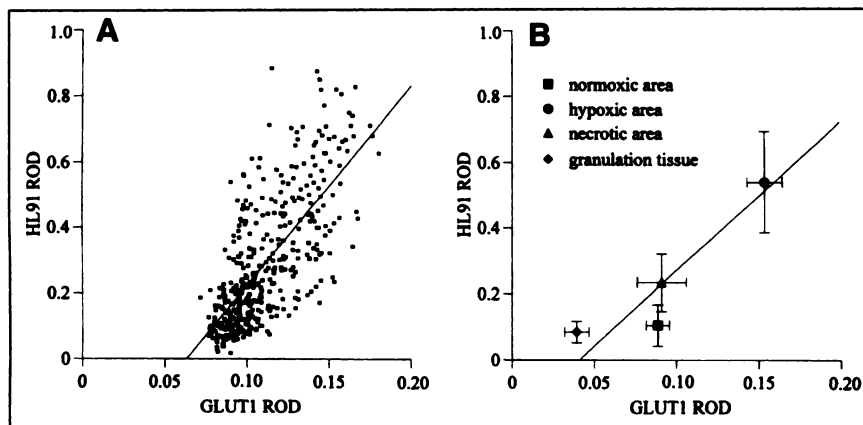
FIGURE 7. (A) Correlation between HL91 uptake and GLUT1 expression in viable cancer cell area of one section (400 data points, r = 0.715, P < 0.0001). (B) Relationship between HL91 uptake and GLUT1 expression in whole section of same sample (740 data points, r = 0.672, P < 0.0001). Data are expressed by each area. Each point was 0.062 mm². Correlations were calculated point by point, and lines were obtained by linear regression.

tinued to increase until 360 min after injection. However, tumor activity was reduced to 50% at 360 min postinjection because of the short half-life of ^{99m}Tc. Thus, we decided to kill rats for autoradiography 240 min after injection of HL91. Uptake of DG by tumor reached a peak 90 min after injection and then gradually decreased. The tumor-to-muscle ratios reached a peak at 60 min and then decreased gradually, whereas the tumor-to-blood ratios continued to increase until 180 min. On the basis of these results, we decided to kill rats for autoradiography 90 min after injection of DG.

HL91 has shown similar tumor-to-muscle and tumor-to-blood ratios to hypoxia tracers FMISO and IAZA at 2 h after injection (18,21). However, HL91 has the advantages of being easily prepared from a kit and low cost. Ballinger et al. (28) reported that slow blood clearance of BMS181321 caused low tumor-to-blood ratios. Extensive hepatobiliary clearance of BMS18132, with resulting high levels of background activity in the abdomen, was also shown. On the other hand, in this study, HL91 showed rapid blood clearance and a high tumor-to-blood ratio; HL91 also showed a higher tumor-to-muscle ratio than BMS181321. These re-

sults suggest that tumor tissue may be more effectively visualized by HL91 than by BMS181321, although the tumor cell and the host used in this study were different from those used in the study of Ballinger et al. Furthermore, HL91 has the additional advantage of being excreted primarily through the kidneys, whereas most BMS181321 is excreted through the hepatobiliary system.

In this study, uptake of HL91 by the hypoxic area was significantly higher than that by the other areas, indicating that tumor hypoxia may be detected with HL91. We did not measure oxygen tension in this study, and therefore it should be confirmed that there was low oxygen tension in the histologically defined hypoxic area. Uptake of HL91 by the necrotic area was significantly higher than that of the normoxic area. Thus, tumor viability may not be determined by accumulation of HL91.

Brown et al. (32) reported high uptake of FDG and strong expression of GLUT1 in the tumor sites likely to be subjected to hypoxia and found a positive correlation between the in vivo uptake of FDG and staining of GLUT1 antigen in a tumor model. Clavo et al. (33) reported that an increase in FDG uptake and an increase in GLUT1 expres-

TABLE 3
Correlation Between Glucose Transporter (GLUT1) Expression and HL91 or Deoxyglucose (DG) Uptake
in Viable Cancer Cell Area and Whole Section

No. of section	Viable cancer cell area				Whole section			
	GLUT1 vs. HL91		GLUT1 vs. DG		GLUT1 vs. HL91		GLUT1 vs. DG	
	r	n	r	n	r	n	r	n
1	0.829	520	0.451	520	0.695	840	0.275	840
2	0.868	500	0.466	500	0.517	800	0.416	800
3	0.715	400	0.446	400	0.672	740	0.270	740
4	0.624	330	0.576	330	0.508	500	0.384	500
5	0.641	780	0.328	780	0.524	1000	0.288	1000
6	0.753	670	0.616	670	0.663	840	0.246	840
7	0.673	630	0.607	630	0.634	860	0.228	860
8	0.726	640	0.669	640	0.460	810	0.335	810
Mean r	0.743		0.505		0.607		0.303	

n = number of points.
P < 0.0001 in all cases. Data represent eight sections from eight rats.

FIGURE 8. (A) Correlation between DG uptake and GLUT1 expression in viable cancer cell area of one section (400 data points, $r = 0.466$, $P < 0.0001$). (B) Relationship between DG uptake and GLUT1 expression in whole section of same sample (740 data points, $r = 0.270$, $P < 0.0001$). Data are expressed by each area. Each point was 0.062 mm^2. Correlations were calculated point by point, and line in (A) was obtained by linear regression.
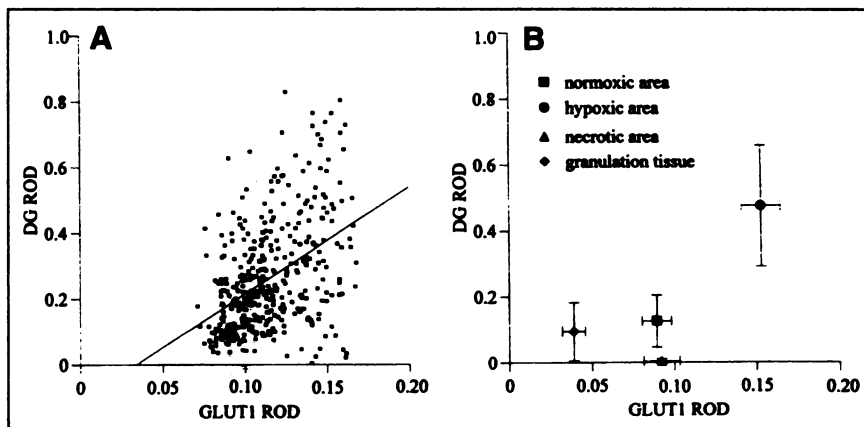
sion were found in HTB77 IP3 cells (in vitro) after exposure to an atmosphere of low oxygen. Loike et al. (*34*) reported that hypoxia induced the expression of GLUT1 mRNA and protein in endothelial cells. In the present study, uptake of HL91 and DG, and the expression of GLUT1 in the hypoxic area were significantly higher than those in the normoxic area. Good correlation was found between the uptake of HL91 and the expression of GLUT1 in the viable cancer cell area, suggesting that hypoxia increases the expression of GLUT1 and the accumulation of HL91 in viable cancer cells. There was also a significant correlation between the uptake of DG and GLUT1 antigen staining in the viable cancer cell area, but the expression of GLUT1 correlated better with the uptake of HL91 than with DG uptake ($P < 0.01$). Moreover, uptake of DG in the hypoxic area was generally high but variable. Although hypoxia may increase the expression of GLUT1, DG uptake may not be determined only by the amount of GLUT1 expressed in the viable cancer cells. In addition to transmembrane transport, regional blood flow in tumor tissue and rates of intracellular phosphorylation and dephosphorylation will affect the DG uptake (*35*). Correlation was moderate between the uptake of HL91 and the staining of GLUT1 antigen by the whole tumor section, whereas no correlation between the uptake of DG and the staining of GLUT1 antigen was observed. A whole tumor section contains not only viable cancer cells but noncancerous components such as granulation tissue. In addition, some necrotic cancer cells and debris in the necrotic area were strongly stained by anti-GLUT1 antibody. These results may explain the difference in the correlation between the viable cancer cell area and the whole tumor section.

CONCLUSION

High tumor-to-muscle and tumor-to-blood ratios were obtained in this biodistribution study of HL91. HL91 accumulated to significantly higher levels in the hypoxic area than in other tissues. In the viable cancer cell area, uptake of HL91 was strongly correlated with expression of GLUT1. These results indicate that HL91 can be used to detect tumor hypoxia.

REFERENCES

1. Gatenby RA, Coia LR, Richter MP, et al. Oxygen tension in human tumors: in vivo mapping using CT-guided probes. *Radiology.* 1985;156:211–214.
2. Vaupel P, Schlenger K, Knoop C, Höckel M. Oxygenation of human tumors: evaluation of tissue oxygen distribution in breast cancers by computerized O_2 tension measurements. *Cancer Res.* 1991;51:3316–3322.
3. Gatenby RA, Kessler HB, Rosenblum JS, et al. Oxygen distribution in squamous cell carcinoma metastases and its relationship in outcome of radiation therapy. *Int J Radiat Oncol Biol Phys.* 1988;14:831–838.
4. Höckel M, Knoop C, Schlenger K, Vorndran B, Knapstein PG, Vaupel P. Intratumoral pO_2 histography as predictive assay in advanced cancer of the uterine cervix. In: Vaupel P, et al., eds. *Oxygen transport to tissue XV.* New York, NY: Plenum; 1994:445–450.
5. Vanderkooi JM, Erecinska M, Silver IA. Oxygen in mammalian tissue: methods of measurement and affinities of various reactions. *Am J Physiol.* 1991;260:C1131–C1150.
6. Nunn A, Linder K, Strauss HW. Nitroimidazoles and imaging hypoxia. *Eur J Nucl Med.* 1995;22:265–280.
7. Martin GV, Caldwell JH, Rasey JS, Grunbaum Z, Cerqueira M, Krohn KA. Enhanced binding of the hypoxic cell marker [³H]fluoromisonidazole in ischemic myocardium. *J Nucl Med.* 1989;30:194–201.
8. Shelton ME, Dence C, Hwang D-R, Welch MJ, Bergmann SR. Myocardial kinetics of fluorine-18 misonidazole: a marker of hypoxic myocardium. *J Nucl Med.* 1989;30:351–358.
9. Martin GV, Cerqueira M, Caldwell JH, Rasey JS, Embree L, Krohn KA. Fluoromisonidazole: a metabolic marker of myocyte hypoxia. *Circ Res.* 1990;67:240–244.
10. Shelton ME, Dence CS, Hwang D-R, Herrero P, Welch MJ, Bergmann SR. In vivo delineation of myocardial hypoxia during coronary occlusion using fluorine-18 fluoromisonidazole and positron emission tomography: a potential approach for identification of jeopardized myocardium. *J Am Coll Cardiol.* 1990;16:477–485.
11. Martin GV, Caldwell JH, Graham MM, et al. Noninvasive detection of hypoxic myocardium using fluorine-18-fluoromisonidazole and positron emission tomography. *J Nucl Med.* 1992;33:2202–2208.
12. Martin GV, Biskupiak JE, Caldwell JH, Rasey JS, Krohn KA. Characterization of iodovinylmisonidazole as a marker for myocardial hypoxia. *J Nucl Med.* 1993;34:918–924.
13. Chapman JD. Hypoxic sensitizers: implications for radiation therapy. *N Engl J Med.* 1979;301:1429–1432.
14. Rasey JS, Krohn KA, Grunbaum Z, Conroy PJ, Bauer K, Sutherland RM. Further characterization of 4-bromomisonidazole as a potential detector of hypoxic cells. *Radiat Res.* 1985;102:76–85.
15. Urtasun RC, Chapman JD, Raleigh JA, Franko AJ, Koch CJ. Binding of ³H-misonidazole to solid human tumors as a measure of tumor hypoxia. *Int J Radiat Oncol Biol Phys.* 1986;12:1263–1267.

16. Rasey JS, Koh W-J, Grierson JR, Grunbaum Z, Krohn KA. Radiolabeled fluoromisonidazole as an imaging agent for tumor hypoxia. *Int J Radiat Oncol Biol Phys.* 1989;17:985–991.

17. Koh W-J, Rasey JS, Evans ML, et al. Imaging of hypoxia in human tumors with [F-18]fluoromisonidazole. *Int J Radiat Oncol Biol Phys.* 1992;22:199–212.

18. Mannan RH, Somayaji VV, Lee J, Mercer JR, Chapman JD, Wiebe LI. Radioiodinated 1-(5-iodo-5-deoxy-β-D-arabinofuranosyl)-2-nitroimidazole (iodo-azomycin arabinoside: IAZA): a novel marker of tissue hypoxia. *J Nucl Med.* 1991;32:1764–1770.

19. Parliament MB, Chapman JD, Urtasun RC, et al. Non-invasive assessment of human tumour hypoxia with ^{123}I-iodoazomycin arabinoside: preliminary report of a clinical study. *Br J Cancer.* 1992;65:90–95.

20. Groshar D, McEwan AJB, Parliament MB, et al. Imaging tumor hypoxia and tumor perfusion. *J Nucl Med.* 1993;34:885–888.

21. Yang DJ, Wallace S, Cherif A, et al. Development of F-18-labeled fluoroerythro-nitroimidazole as a PET agent for imaging tumor hypoxia. *Radiology.* 1995;194:795–800.

22. Rumsey WL, Cyr JE, Raju N, Narra RK. A novel [99m]technetium-labeled nitroheterocycle capable of identification of hypoxia in heart. *Biochem Biophys Res Commun.* 1993;193:1239–1246.

23. Kusuoka H, Hashimoto K, Fukuchi K, Nishimura T. Kinetics of a putative hypoxic tissue marker, technetium-99m-nitroimidazole (BMS181321), in nor-moxic, hypoxic, ischemic and stunned myocardium. *J Nucl Med.* 1994;35:1371–1376.

24. Stone CK, Mulnix T, Nickles RJ, et al. Myocardial kinetics of a putative hypoxic tissue marker, ^{99m}Tc-labeled nitroimidazole (BMS181321), after regional isch-emia and reperfusion. *Circulation.* 1995;92:1246–1253.

25. Rumsey WL, Patel B, Linder KE. Effect of graded hypoxia on retention of technetium-99m-nitroheterocycle in perfused rat heart. *J Nucl Med.* 1995;36:632–636.

26. Shi CQ, Sinusas AJ, Dione DP, et al. Technetium-99m-nitroimidazole (BMS181321): a positive imaging agent for detecting myocardial ischemia. *J Nucl Med.* 1995;36:1078–1086.

27. Fukuchi K, Kusuoka H, Watanabe Y, Fujiwara T, Nishimura T. Ischemic and reperfused myocardium detected with technetium-99m-nitroimidazole. *J Nucl Med.* 1996;37:761–766.

28. Ballinger JR, Kee JWM, Rauth AM. In vitro and in vivo evaluation of a technetium-99m-labeled 2-nitroimidazole (BMS181321) as a marker of tumor hypoxia. *J Nucl Med.* 1996;37:1023–1031.

29. Archer CM, Edwards B, Kelly JD, King AC, Burke JF, Riley ALM. Technetium labeled agents for imaging tissue hypoxia in vivo. In: Nicolini M, Bandoli G, Mazzi U, eds. *Proceedings of the Fourth International Symposium on Technetium in Chemistry and Nuclear Medicine.* Padova, Italy: SGE Ditoriali; 1995:535–539.

30. Okada RD, Johnson G III, Nguyen KN, Edwards B, Archer CM, Kelly JD. ^{99m}Tc-HL91 effects of low flow and hypoxia on a new ischemia-avid myocardial imaging agent. *Circulation.* 1997;95:1892–1899.

31. Cook GJR, Houston S, Barrington SF, Fogelman I. Technetium-99m-labeled HL91 to identify tumor hypoxia: correlation with fluorine-18-FDG. *J Nucl Med.* 1998;39:99–103.

32. Brown RS, Leung JY, Fisher SJ, Frey KA, Ethier SP, Wahl RL. Intratumoral distribution of tritiated-FDG in breast carcinoma: correlation between GLUT-1 expression and FDG uptake. *J Nucl Med.* 1996;37:1042–1047.

33. Clavo AC, Brown RS, Wahl RL. Fluorodeoxyglucose uptake in human cancer cell lines is increased by hypoxia. *J Nucl Med.* 1995;36:1625–1632.

34. Loike JD, Cao L, Brett J, Ogawa S, Silverstein SC, Stern D. Hypoxia induces glucose transporter expression in endothelial cells. *Am J Physiol.* 1992;263:C326–C333.

35. Rigo P, Paulus P, Kaschten BJ, et al. Oncological applications of positron emission tomography with fluorine-18 fluorodeoxyglucose. *Eur J Nucl Med.* 1996;23:1641–1674.